Tan, C. M., Fletcher, P. N., Beach, M. A., Nix, A. R., Landmann, M., & Thoma, R. S. (2002). On the application of circular arrays in direction finding. Part I: Investigation into the estimation algorithms. (pp. 16 p). (COST 273), (WP 02 007).

On the Application of Circular Arrays in Direction Finding Part I: Investigation into the estimation algorithms

C. M. Tan[1,†], P. Fletcher[2], M. A. Beach[1], A. R. Nix[1], M. Landmann[3], and R. S. Thomä[3]

[1]Centre for Communications Research,
Dept. Electrical and Electronic Eng.,
University of Bristol,
Bristol BS8 1UB, UK.
Tel: +44 117 954 5202
Fax: +44 117 954 5206

[2]QinetiQ
St. Andrew's Road, Malvern,
Worcs, WR14 3PS,
UK.
Tel: +44 117 954 5390
Fax: +44 117 954 5206

[3]Technical University Ilmenau,
Dept. Communication and Measurement,
P.O. Box 100565,
98684 Ilmenau, Germany.
Tel: +49 3677 69 1157
Fax: +49 3677 69 1113

[†]Email: Chor.Min.Tan@bristol.ac.uk

ABSTRACT

The performance of different direction finding algorithms for the circular arrays is investigated in this paper. Several direction estimation algorithms are studied with their pros and cons discussed. Special consideration is given to the necessary conditions needed prior to applying the algorithms in order to guarantee high accuracy in the field. Their performance is evaluated based on a simplified data model with some further assumptions, and followed by a top level comparison between each of the algorithms. The on-going research shows that the performance of the SAGE is superior to any of the other algorithms considered here when applied to a circular array.

I. INTRODUCTION

Numerous research activities have focused on evaluating the spatial characteristics of the radio channel such that antenna array based systems can be optimised during design. One of the major parameters available from the spatial domain is that of directional information, thus estimating the direction-of-arrival (DoA) or direction-of-departure (DoD) of multipaths has received considerable attention.

Different direction finding techniques and algorithms have been developed leading to significant improvements in DoA estimation over the last decade. However, to date, most of the reported algorithms are based on the uniform linear array (ULA) and the uniform rectangular array (URA) architectures, and very little attention has been given to the circular array topologies despite of their ability to offer a number of advantages. A uniform circular array (UCA) is able to provide 360º azimuthal coverage and a certain degree of source elevation information (depending on its element beampattern). Note that a URA with non-omnidirectional elements is not able to provide full azimuthal coverage due to the directional beampattern of its elements. In a beamforming application, the directional patterns of a UCA can be electronically rotated throughout the azimuth without significant change in the beam shape. All elements on the UCA will exhibit identical beampattern since the UCA has no edge elements and is less sensitive to the mutual coupling effects (compared to ULA and URA).

In terms of radio propagation, especially in a multipath-rich environment, the signals will arrive at the mobile terminal potentially from any azimuth direction. Using a ULA in a channel sounding campaign in this case will restrict the azimuth field of view to less than 180º (typically 120º). A short-term solution to this is to use several ULAs arranged in a triangular or rectangular shape (Figure 1), or to rotate the ULA a few times in order to cover the full azimuth spread. However, the drawback for the former solution is the requirement of using several ULAs (hence increasing the cost) as well as collecting additional data. While in latter solution, the time for recording the full azimuth responses will be more than the coherence time of a non-stationary channel. Obviously, the problem becomes more complicated in a double-directional measurement needed to simulate the ad-hoc channel where each mobile terminal will also act as a basestation and full azimuthal coverage is required at both ends.

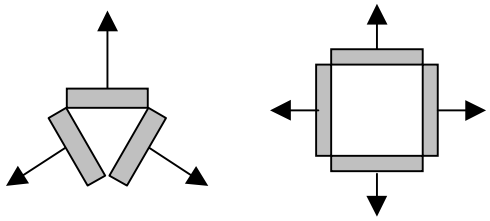

Figure 1 Triangular and rectangular arrangement of the ULAs, each covering 120º and 90º field of view

Therefore, the UCA plays an important role and its application in direction finding is investigated in this paper. Part I of this paper is organised as follows. A brief study on the UCA phase-mode excitation is given in Section 2. Section 3 investigates the pros and cons of several DoA estimation algorithms, followed by the general discussions on various issues in Section 4. Finally, Section 5 concludes Part I. In Part II [1], we evaluate the performance of the Space-Alternating Generalised Expectation-maximisation (SAGE) algorithm with real measurement data using different UCAs.

II. PHASE-MODE EXCITATION[1]

Since the beampattern of the UCA is periodic in azimuth, it can be broken down into different Fourier harmonics by using the Fourier analysis. Each of these Fourier harmonics is termed a phase-mode of the UCA [2]. The phase-mode excitation is able to transform the UCA array manifold (in the element space) into the ULA-like manifold in the UCA's phase-mode space [3]. Thus, most of the normal ULA signal processing methods (e.g. Butler beamforming matrices) can be applied to the UCA in the phase-mode domain provided certain conditions are met.

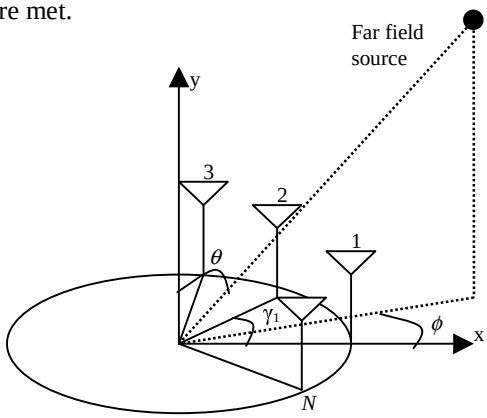

Figure 2 Uniform circular array geometry

Figure 2 shows the geometry of an *N*-element omni-directional UCA, where $\gamma_n = 2\pi n/N$, θ and ϕ are the source polar and azimuth angles measured from the *y* and *x* axis, respectively. Taking the centre of the UCA as reference, the phase shift experienced by the *n*-th element caused by a far field source is given by

$$a_n(\Theta) = e^{jk_0 r \sin\theta \cos(\phi - \gamma_{n-1})} \qquad (1)$$

$n \in [1,N]$, and the array steering vector is

$$a(\Theta) = [a_1(\Theta), a_2(\Theta), \cdots\cdots, a_N(\Theta)]^T \qquad (2)$$

where *T* denotes the vector transposition, *r* is the UCA radius, $k_0 = 2\pi/\lambda$, λ is the wavelength of the radiated signal, and $\Theta = (\theta, \phi)$.

The UCA can be excited with *m*-th phase-mode by using a *m*-th phase-mode beamforming vector, w_m:

$$w_m = \frac{1}{N}\left[e^{-jm\gamma_0}, e^{-jm\gamma_1}, \ldots\ldots, e^{-jm\gamma_{N-1}}\right]^T \qquad (3)$$

The resulting *m*-th phase-mode array beampattern is

$$f_m(\Theta) = w_m^H a(\Theta) = \frac{1}{N}\sum_{n=0}^{N-1} e^{jm\gamma_n} e^{jk_0 r \sin\theta \cos(\phi - \gamma_n)} \qquad (4)$$

where *H* denotes the Hermitian transpose operator. Using the theorem of the Bessel function,

$$e^{j\beta\cos\alpha} = \sum_{m=-\infty}^{\infty} j^m J_m(\beta) e^{jm\alpha} \qquad (5)$$

where $J_m(\beta)$ denotes a Bessel function of the first kind of order *m* with argument β, (4) can be rewritten as

$$f_m(\Theta) = j^m J_m(k_0 r \sin\theta) e^{jm\phi} + \Delta f_m(\Theta) \qquad (6)$$

where the distortion term, Δf_m, is given by

$$\Delta f_m(\Theta) = \sum_{q=1}^{\infty}\begin{pmatrix} j^g J_g(k_0 r \sin\theta) e^{-jg\phi} + \ldots \\ \ldots j^h J_h(k_0 r \sin\theta) e^{-jh\phi} \end{pmatrix} \qquad (7)$$

where $g = Nq-m$ and $h = Nq+m$.

Note that the original work in phase-mode excitation was based on a circular array with continuous aperture and its *m*-th phase-mode beampattern is given by (6) without the distortion term. For the case of a UCA with discrete elements, since only the first term in (6) is useful, every effort has been made to minimise the distortion term (7) and this has imposed some restrictions in the direction finding algorithms based on the phase-mode excitation.

Two important rules of thumb when applying phase-mode excitation to an *N*-element UCA:

1. From the property of the Bessel function (Figure 3), $J_m(\beta)$ has a small value when $|m|>\beta$. In order to excite the UCA with a reasonable strength using the highest mode *M*, *M* must be $M \approx k_0 r \sin\theta \in [0, k_0 r]$ and the maximum mode is given by the smaller integer that is closer to or equal to $k_0 r$. Hence, the modes that can be excited are $m \in [-M, M]$.

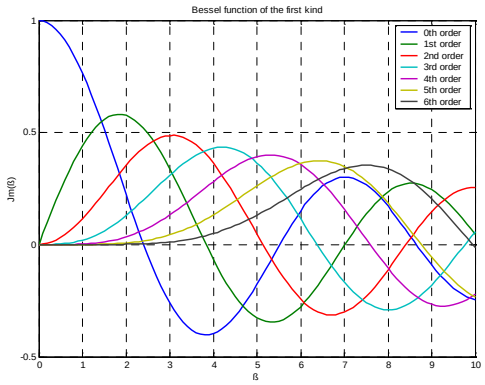

Figure 3 Bessel function of the first kind

2. From the spatial Nyquist sampling theorem, the UCA circumferential sampling rate should be at least twice the highest spatial frequency present in the array excitation [2]. Therefore, in order to reproduce all the spatial harmonics that are

[1] The concept of the phase-mode excitation of a UCA was introduced in the 1960s and had been studied in great depth by Davies [2][3].

excited, the number of elements in the UCA must satisfy $N \geq 2M$.

Note that these two conditions decide the appropriate radius and number of elements of the UCA, and thus set the largest circumferential spacing between the adjacent UCA elements to be $\lambda/2$, and $r_{\max} = \frac{N\lambda}{4\pi}$.

III. INVESTIGATION INTO DIFFERENT DIRECTION FINDING ALGORITHMS

This section investigates several direction finding algorithms using a UCA. To aid the following discussions, we begin by constructing a common narrowband signal model used in the estimation algorithms. Assuming a total of *K* sources impinging on an *N*-element omni-directional UCA, the array response can be represented by

$$x(t) = As(t) \qquad (8)$$

where $A = [a(\Theta_1) : a(\Theta_2) : \cdots\cdots : a(\Theta_K)]$ is the array response matrix, and $s(t) = [s_1(t), s_2(t), \cdots\cdots, s_K(t)]^T$ represents the *K* far field sources. In order to simplify the studies, it is assumed that the number of sources is known, the sources are uncorrelated, the channel is noiseless, and the sources lie in the azimuth plane, i.e. $\theta = 90^o$ and $\Theta \equiv \phi$.

A number (*p*) of array snapshots are collected within the coherence time of the channel and the data matrix is given by

$$X = [x(t_1) : x(t_2) : \cdots\cdots : x(t_p)] \qquad (9)$$

The expected covariance matrix, *R*, is thus defined as

$$R = \frac{1}{p} XX^H \qquad (10)$$

A. The Classical Beamforming Method (CBM)

The CBM is the simplest direction finding algorithm. It estimates the DoA of the signals by scanning a beam throughout the azimuth, and the DoAs are located by the peaks in the power azimuth spectrum, $P_{CBM}(\phi)$, given by

$$P_{CBM}(\phi) = a^H(\phi) R a(\phi) \qquad (11)$$

Similar to the ULA's case, the performance of CBM is limited by the Rayleigh resolution and is not able to resolve the closely spaced signals.

B. Capon's Beamforming Method (Min-Variance)

The Capon's Beamforming [4] method is also known as the Minimum Variance Distorsionless Response (Min-Variance). It is similar to the CBM, with an additional feature of minimising the power contributed by signals from other direction while maintaining a fixed gain in the look direction. Although its resolution is better than CBM, it is still dependent upon the number of elements and the signal-to-noise ratio (SNR) of the channel. Its power azimuth spectrum is given by

$$P_{MV}(\phi) \frac{1}{a^H(\phi) R^{-1} a(\phi)} \qquad (12)$$

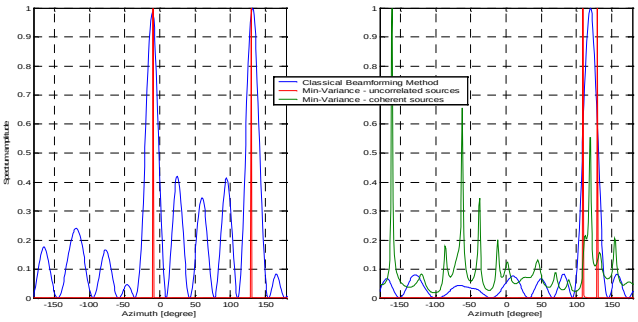

a *b*

a – 2 equipower uncorrelated sources at -10º and 130º
Classical Beamforming Method, Min-Variance

b – 2 equipower sources at 110º and 130º
Classical Beamforming Method (uncorrelated sources)
Min-Variance (uncorrelated sources)
Min-Variance (sources are coherent)

16-element omni-directional UCA, r=λ

Figure 4 Power spectrums of the CBM and Min-Variance algorithm

Figure 4 (details in caption) demonstrates the poor resolution of the CBM that is not able to resolve closely spaced sources. The high sidelobes of the CBM also leads to misleading results. Although Min-Variance has high-resolution, it fails when the sources are coherent.

C. MUltiple SIgnal Classification (MUSIC)

C.1. Conventional MUSIC in element space

Although the element space MUSIC algorithm introduced by Schmidt [5] has been widely used with a ULA, it can also be used with a UCA, provided that the sources are uncorrelated and the knowledge of array manifold is available. Using the eigen-decomposition procedure explained in [5], the MUSIC spectrum is given by

$$P_{MU}(\phi) = \frac{1}{a^H(\phi) E E^H a(\phi)} \qquad (13)$$

where *E* is the noise subspace of *R* in (10), and $a(\phi)$ is defined in (2).

C.2. MUSIC in phase-mode space

When the sources are coherent, the covariance matrix *R* is rank deficient and spatial smoothing technique

must be applied prior to applying any eigen-decomposition based algorithm. However, the original development of the spatial smoothing technique [6] was based on the Vandermonde structure in the steering vector of a ULA. UCA phase-mode excitation provides a means to restore the Vandermonde structure in the UCA steering vector (2), with the penalty of reduced aperture size in the phase-mode space.

C.2.1. Standard implementation

The element space data matrix, X, can be transformed into the phase-mode space by

$$X_{pm} = JF^H X \qquad (14)$$

where

$$J = diag\left\{\frac{1}{\sqrt{N}\, j^m J_m(k_0 r)}\right\} \; m \in [-M, M] \qquad (15)$$

and $$F = [w_{-M} \vdots \cdots\cdots \vdots w_0 \vdots \cdots\cdots \vdots w_M] \qquad (16)$$

is the phase-mode beamforming matrix. At this stage, the UCA spatial smoothing [7] technique can be applied to the new phase-mode space data (14).

For simplicity, without applying the phase-mode spatial smoothing, the MUSIC spectrum is given by

$$P_{pm}(\phi) = \frac{1}{a_{pm}^H(\phi) E_{pm} E_{pm}^H a_{pm}(\phi)} \qquad (17)$$

where E_{pm} is the phase-mode space noise-subspace, and $a_{pm}(\phi) = JF^H a(\phi)$ is the phase-mode steering vector that exhibits the Vandermonde structure.

Note that the Bessel function term, $J_m(.)$, has been included in the computation of J in (15), since we have assumed $\theta = 90^o$ here. However, as $\theta \neq 90^o$ in practice, $J_m(.)$ would not be included in (15) so that θ can be estimated as well.

C.2.2. UCA-RB-MUSIC

The UCA Real Beamspace MUSIC (UCA-RB-MUSIC) introduced by Mathews and Zoltowski [8] transforms the data matrix and the array manifold into their real-valued counterparts in phase-mode space by using a unitary matrix W (refer to [8] for the construction of W). Due to the property of W, UCA-RB-MUSIC effectively works with a forward-backward averaged covariance matrix. Hence, its performance is more robust when dealing with two correlated sources. However, when more than two sources are correlated, spatial smoothing [7] must be applied. In addition, in the case of estimating both θ and ϕ, the speed of locating the peaks in its 2-D spectrum can be accelerated with the aid of a FFT process (more details in [8]).

C.2.3. Unitary UCA-MUSIC

Note that the noise subspace in the UCA-RB-MUSIC is determined from the real part of the calculated covariance matrix. This is rather confusing since the computation in UCA-RB-MUSIC is accomplished in real-valued space. The authors [8] had claimed that the UCA-RB-MUSIC is implemented in real-valued since its imaginary part is nearly zero, i.e. almost real. In order to fully eliminate the imaginary part to facilitate the real-valued eigen-decomposition, the authors had ignored the 'nearly-zero' imaginary part of the covariance matrix. To some small extent, this leads to minor leakage of some useful information associated with the imaginary part.

Enhancement can be made by using the unitary left Π-real matrix defined in [9] – 'Q', to convert the complex-valued data matrix into its real-valued counterpart in phase-mode space. Hence, the eigen-decomposition of the covariance matrix in Unitary UCA-MUSIC can be performed in a true real-valued domain. Similarly, the forward-backward averaging process has been incorporated in this process and hence, the Unitary UCA-MUSIC is also robust in resolving two correlated sources.

C.3. Simple demonstration on MUSIC

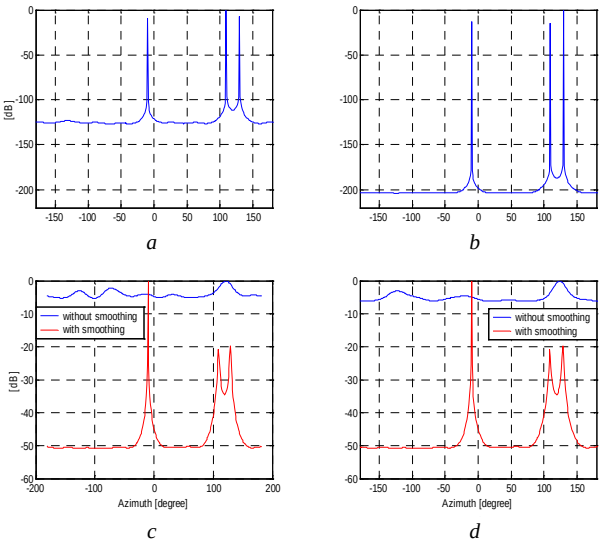

a – spectrum of UCA-RB-MUSIC
b – spectrum of Unitary UCA-MUSIC
c – spectrums of phase-mode space MUSIC
d – spectrums of Unitary UCA-MUSIC

16-element omni-directional UCA, r = λ
without smoothing, with smoothing
a, b – 3 equipower uncorrelated sources at -10º, 110º, 130º
c, d – 3 equipower coherent sources at -10º, 110º, 130º

Figure 5 Spectrums of various MUSIC algorithms

From the spectrums of UCA-RB-MUSIC and Unitary UCA-MUSIC algorithms shown in Figures 5a and 5b respectively (details in caption), the performance of UCA-RB-MUSIC is inferior to that

of Unitary UCA-MUSIC since the latter has a lower noise floor. Nevertheless, both algorithms have successfully produced the correct estimates and the peaks corresponding to the three sources can be easily located. The total failure of the algorithms without spatial smoothing shown in Figures 5c and 5d demonstrates that spatial smoothing process must be performed when the sources are coherent.

D. Estimation of Signal Parameters via Rotational Invariance Techniques (ESPRIT)

One strict condition imposed by ESPRIT [10] is the presence of two identical, translationally invariant subarrays. Although we can define two such subarrays from a UCA, Swindlehurst [11] showed that the original ESPRIT [10] algorithm applied to UCA fails when more than one source is present. Therefore, special modifications must be performed if ESPRIT were to be used with a UCA.

D.1. UCA-ESPRIT

Mathews and Zoltowski [8][12] had proposed the UCA-ESPRIT algorithm based on the concept of recursive relationship of the Bessel functions:

$$J_{m-1}(\beta)+J_{m+1}(\beta)=\frac{2m}{\beta}J_m(\beta) \qquad (18)$$

Although its implementation is a little different from the original ESPRIT, it is similar in the sense that a Least Squares solution must be performed on a set of overdetermined equations before the signal parameters are obtained from its eigenvalues. The main advantage of UCA-ESPRIT is its ability to provide automatically paired θ and ϕ as a closed-form solution. However, in a non-coherent case, the maximum number of sources that can be resolved is M-1, i.e. less than half of the resolution of MUSIC. Moreover, its estimates are also a little biased. Hence, the authors had proposed to use the UCA-ESPRIT to provide a coarse estimate to initialise the search function of the MUSIC in order to increase the convergence speed of the MUSIC's peak-searching routine.

Table 1 shows the results of UCA-ESPRIT under different conditions (details in caption). The number of sources that can be resolved by UCA-ESPRIT when N = 8 is 2, since $M_{(N=8)}$ = 3. By using a UCA with more elements, the number of resolvable sources can be increased and the estimates are also more accurate, since the degree of freedom is higher. This is shown in Table 1 where the estimated results when N = 16 are more accurate. In addition, by using a UCA with its radius smaller than the upper bound limit stated in Section 2, i.e. circumferential spacing between adjacent elements of less than $\lambda/2$, the accuracy of the estimates can also be improved.

N	r [λ]	$(\theta_1, \phi_1) = (75^o, 110^o)$ $(\theta_2, \phi_2) = (90^o, 130^o)$
8	0.63	$\Theta_{e1} = (45^o, 108.7^o)$ $\Theta_{e2} = (90^o, 125.5^o)$
	0.50	$\Theta_{e1} = (72^o, 105.0^o)$ $\Theta_{e2} = (90^o, 126.6^o)$
16	1.27	$\Theta_{e1} = (69^o, 108.7^o)$ $\Theta_{e2} = (90^o, 135.5^o)$
	1.00	$\Theta_{e1} = (78^o, 110.8^o)$ $\Theta_{e2} = (90^o, 131.3^o)$

N-element omni-directional UCA with r radius [in terms of λ]
2 equipower uncorrelated sources at (75º, 110º) and (90º, 130º)
Estimated direction is shown in third column by Θ_{e1} *and* Θ_{e2}

Table 1 Estimated results using UCA-ESPRIT

D.2. Unitary UCA-ESPRIT in phase-mode space

Similar to the UCA-RB-MUSIC, the process of eigen-decomposition of the covariance matrix in UCA-ESPRIT has ignored the 'nearly-zero' imaginary part of its covariance matrix. In order to facilitate a true real-valued computation, and to improve the resolution of UCA-ESPRIT, the Unitary UCA-ESPRIT in phase-mode space is proposed here.

The implementation of Unitary UCA-ESPRIT is based on the combined concept of phase-mode excitation and Unitary ESPRIT [9] algorithm. Similar to the Unitary UCA-MUSIC algorithm, the new introduced step in Unitary UCA-ESPRIT involves the transformation of the phase-mode space data matrix (14) from its complex space to its real-valued counterpart by using the unitary left Π-real matrix defined in [9] – 'Q', and followed by the ordinary Unitary ESPRIT procedure in the subsequent steps. This results in increased accuracy compared to UCA-ESPRIT, and increased number of resolvable uncorrelated sources from M-1 to 2M.

However, since the θ-dependent term, i.e. the Bessel function, has been eliminated by J (15) in X_{pm} (14), only azimuth angle can be estimated using the Unitary UCA-ESPRIT algorithm. This also suggests a degradation in the performance of Unitary UCA-ESPRIT if $\theta \neq 90^o$, and from the extensive simulation results, Unitary UCA-ESPRIT fails when $\theta < 70^o$. This implies that although the performance of Unitary UCA-ESPRIT is superior to UCA-ESPRIT when $\theta = 90^o$, UCA-ESPRIT would still be the preferred choice since $\theta \neq 90^o$ in practice.

D.3. CUBA-ESPRIT

The CUBA-ESPRIT [13] was specially developed for direction finding using a circular uniform beam array [14] (CUBA). Its implementation requires that the element beampattern of the array exhibit a $sinc(x)$ function, or more precisely the beam spectrum must

be bandlimited. Figure 6 shows the beampattern of an 8-element CUBA and one of its elements. Due to the unique feature of this *sinc*(*x*)-shape pattern, the CUBA element space data can be transformed into a virtual aperture domain by an FFT process, in which the shift invariance property of the ESPRIT is fully restored, and the spatial smoothing process can thus be applied. This advantage is achieved at a cost of a smaller virtual aperture size and hence a reduction in the total number of resolvable sources.

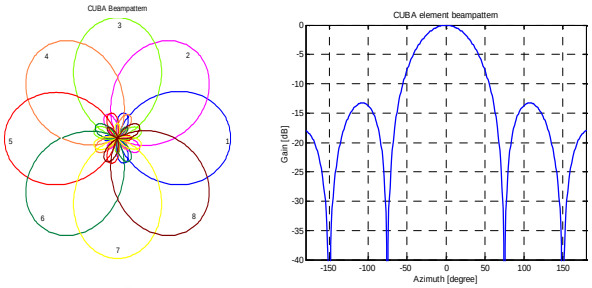

a *b*

a – 8-element CUBA beampattern
b – Beampattern for the 1st element

Figure 6 CUBA beampattern

For the case of a UCA, if the beampattern does not exhibit the appropriate *sinc*(*x*) function, a *sinc*(*x*) beamforming procedure can be performed prior to implementing the CUBA-ESPRIT. However, due to all sorts of array imperfections, a perfect *sinc*(*x*)-shape beampattern could not be synthesised even after the beamforming procedure and this leads to increased bias and errors in the estimation.

In addition, CUBA-ESPRIT assumes that there is no additional phase shift at the element-outputs, i.e. a common phase centre for all elements. This implies that the UCA must have very small diameter (ideally zero) like that of a CUBA, which is practically impossible for a normal UCA. Although CUBA-ESPRIT has been proven to be very efficient and robust, it is only suitable for a CUBA but not for other ordinary UCAs, especially for those with directional element beampattern.

E. Space-Alternating Generalised Expectation-maximisation (SAGE)

Similar to the Expectation-Maximisation (EM) algorithm [15], the SAGE algorithm [16][17] is a maximum-likelihood (ML) based algorithm and its implementation is very different from the aforementioned algorithms that rely on eigen-decomposition. Neither does SAGE need to fulfill the rotational invariance characteristic of ESPRIT, nor to exploit the array Vandermonde structure, since spatial smoothing process is not required in SAGE even when the sources are correlated. The principal advantage of SAGE is its flexibility in any array geometry and hence can be applied to any arbitrary array (in theory), provided the knowledge of the array manifold is fully available. However, one major drawback is its slow convergence since it is iterative in nature.

The objective of the SAGE algorithm is to maximise the correlation function, defined as

$$c_k(x,\phi) = x_k^H a(\phi) \qquad (19)$$

where x_k is the *complete data* [15][16] of the *k*-th source. The peak in c_k corresponds to the location of the estimated parameter of the *k*-th source. Figure 7 shows the correlation functions of the SAGE (details in captions). Since this is a 1-D estimation process, the *Serial Interference Cancellation* (SIC) technique proposed in [17] cannot be used, especially in a case where the sources are closely spaced apart. Here, we have used the conventional *Parallel Interference Cancellation* (PIC) technique [16].

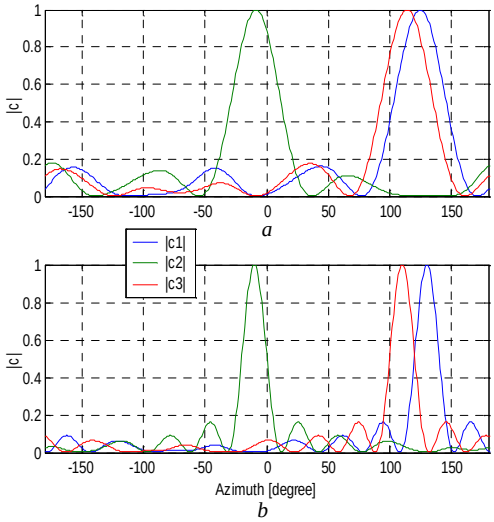

a

b

a – 8-element omni-directional UCA, r=λ/2
b – 16-element omni-directional UCA, r=λ
3 equipower coherent sources at -10º, 110º, 130º
correlation function for the 130º source
correlation function for the -10º source
correlation function for the 110º source

Figure 7 Correlation functions of the SAGE with PIC technique

As shown here, SAGE is able to cope with the coherent sources and spatial smoothing is not required. The convergence speed of SAGE depends on the degree of separation between the paths, and the number of elements used in the array, since the number of samples required in the correlation increases (more samples can enhance the accuracy of the correlation) as the number of elements increases. For a 16-element UCA, the SAGE has converged after 3 iterations, giving the correct estimates at -10º, 110º, and 130º (Figure 7b). However, for the 8-element UCA, after 3 iterations, the estimated results are -9º, 114º, and 125º (Figure 7a) and thus more iterations are needed to achieve convergence especially for the 2 sources at 110º and 130º. Note that in practice, more iterations might be needed since we have assumed a simplified model here. In

any event, as the number of samples grows, the computational load of the SAGE increases exponentially especially in a multi-dimensional case.

F. UCA-to-ULA mapping technique

The so-called '*mapping*' technique proposed by Hyberg [18] can transform the UCA data, in a Least Squares sense, into that of a virtual ULA, by a transformation matrix - T_k. The computation of T_k requires a large amount of measured array manifold data and can only map a small sector (typically 30º as recommended) of a UCA data onto the virtual ULA each time.

After the UCA-to-ULA mapping, both the θ and ϕ are estimated using the normal ULA-type algorithms separately in the transformed elevation and azimuth domains, respectively. As a result, a separate procedure must be developed to pair up both the θ and ϕ. In addition, Hyberg also reported that biased errors occur in the estimated results using this technique.

In spite of all these problems, Hyberg has claimed that using the similar mapping technique to transform a UCA data into that of a smaller virtual UCA can improve the resolution of the UCA-ESPRIT algorithm.

IV. GENERAL DISCUSSIONS

The effectiveness and performance of the estimation algorithms mainly depend on the array geometry. Most of the array signal processing techniques are based on the ULA since the important criterions needed by the algorithms can be easily fulfilled with a ULA. As such, many researchers have attempted to adapt the ULA's signal processing techniques to the UCA, with some extra procedures like the phase-mode excitation. This causes the original information associated with the UCA to be modified into another domain. However, not all information can be preserved and this leads to degradation in performance. This can be clearly observed in the estimated results of UCA-ESPRIT which is inferior to that of the UCA-MUSIC, where the performance of ESPRIT in ULA is supposed to be superior to MUSIC.

Phase-mode excitation in UCA signal processing is important because it allows the spatial smoothing process to be performed in MUSIC, and the rotational shift invariance property to be restored in ESPRIT. However, the phase-mode excitation for a UCA with discrete elements is distorted by the residue term (7) due to finite sampling around the circular aperture. As the mode being excited becomes larger, the effects caused by the distortion term (7) become more apparent. This is shown in Figure 8 for the 2nd and 7th modes of a 16-element UCA, where the contribution from the distortion term can be clearly seen in the responses of the 7th mode.

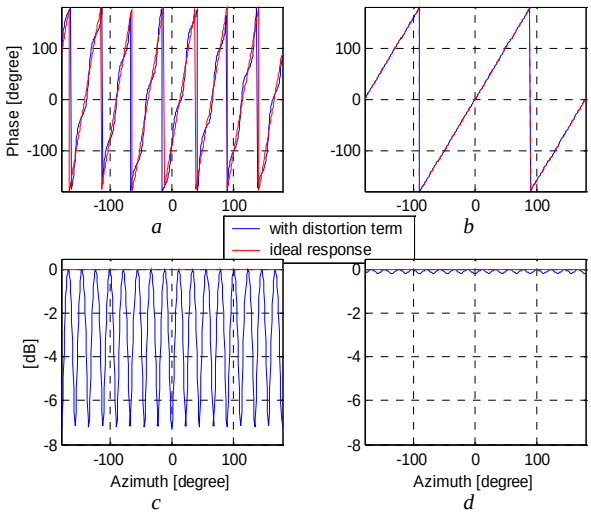

a – phase response of the 7th mode
b – phase response of the 2nd mode
c – amplitude response of the 7th mode
d – amplitude response of the 2nd mode

actual mode response, assumed ideal mode response

Figure 8 Responses of the phase-mode excitation of 16-element omni-directional UCA

In general, using a UCA with $N = 2M + 6$ elements will virtually eliminate the distortion, where M is the maximum mode to be excited [12]. This implies that in order to achieve better accuracy, the transformation from the element space into the phase-mode space has further reduced the aperture size of the data, and hence reducing the maximum number of resolvable sources. This introduces further constraints to the algorithms that a large number of elements is required so that the estimated results will be reliable.

On the other hand, although the SAGE algorithm is computationally expensive (especially in multi-dimensional parameters estimation), it has demonstrated its suitability and excellent performance when applied to a UCA. Chan [19] and Wax [7] showed that the maximum-likelihood algorithms (like SAGE) have better performance than MUSIC. Note that as long as the knowledge of the array manifold is available, SAGE will produce reliable results. The performance of other algorithms considered in this paper is inferior to that of SAGE even when the sources are uncorrelated and the channel is noiseless. One would appreciate further merits on SAGE when the simulation includes highly correlated sources, bad SNR in the channel, and by using a non-ideal UCA with directional beampattern and mutual coupling. Under such conditions, we would expect a total failure in other algorithms but it is very likely that SAGE will survive.

V. CONCLUSION

In this paper, the pros and cons of several direction finding algorithms with a UCA are investigated. The conditions that govern the performance of the algorithms are stated. The analysis shows that the SAGE algorithm is superior to other algorithms when applied to a UCA, and should be the preferred choice when the number of elements is small. Other algorithms are suitable only when the number of elements on the UCA is large, and appropriate spatial calibration algorithm must be performed to eliminate the mutual coupling effects and any array imperfection on the UCA – a process that is essential especially if ESPRIT were to be applied with a UCA.

ACKNOWLEDGEMENT

The authors would like to acknowledge Mobile VCE (www.mobilevce.com) for the financial support of Chor Min Tan.

REFERENCES

[1] C. M. Tan, M. Landmann, A. Richter, L. Pesik, M. A. Beach, Ch. Schneider, R. S. Thomä, A. R. Nix, '*On the application of circular arrays in direction finding, Part 2: Experimental evaluation on SAGE with different circular arrays*', companion paper in 1st Annual COST 273 Workshop, Espoo, Finland, May 29-30, 2002.

[2] D. E. N. Davies, '*Circular arrays*', Chap. 12, The Handbook of antenna design, London Peregrinus on behalf of the IEE, 1983.

[3] D. E. N. Davies, '*A transformation between the phasing techniques required for linear and circular aerial arrays*', Proc. IEE, Vol. 112, No. 11, Nov 1965.

[4] J. Capon, '*High resolution frequency wavenumber spectrum analysis*', Proc. IEEE, Vol. 57, No. 8, Aug 1969, pp. 1408-1418.

[5] R. O. Schmidt, '*Multiple emitter location and signal parameters estimation*', IEEE Trans. Ant. Prop., Mar 86, pp. 276-280.

[6] T. J. Shan, M. Wax, T. Kailath, '*On spatial smoothing for direction-of-arrival estimation of coherent signals*', IEEE Trans. ASSP, Vol. 33, Aug 1985, pp. 806-811.

[7] M. Wax, J. Sheinvald, '*Direction finding of coherent signals via spatial smoothing for uniform circular arrays*', IEEE Trans. Ant. Prop., Vol. 42, No. 5, May 1994, pp. 613-620.

[8] C. P. Mathews, M. D. Zoltowski, '*Eigenstructure techniques for 2-D angle estimation with uniform circular arrays*', IEEE Trans. Signal Proc., Vol. 42, No. 9, Sept 1994, pp. 2395-2407.

[9] M. Haardt, J. A. Nossek, '*Unitary ESPRIT: How to obtain increased estimation accuracy with a reduced computational burden*', IEEE Trans. Signal Proc., Vol. 43, May 1995, pp. 1232-1242.

[10] R. Roy, T. Kailath, '*ESPRIT-Estimation of Signal Parameters via Rotational Invariance Techniques*', IEEE Trans. ASSP, Vol. 37, pp. 984-995, July 1989.

[11] A. Swindlehurst, '*DOA identifiablity for rotationally invariant arrays*', IEEE Trans. Signal Proc., Vol. 40, No. 7, July 1992, pp. 1825-1827.

[12] C. P. Mathews, M. D. Zoltowski, '*Performance analysis of the UCA-ESPRIT algorithm for circular ring arrays*', IEEE Trans. Signal Proc., Vol. 42, No. 9, Sept 1994, pp. 2535-2539.

[13] A. Richter, R. S. Thomä, '*CUBA-ESPRIT for angle estimation with circular uniform beam arrays*', Proc. Millennium Conf. AP2000, Davos, Switzerland, Apr 9-14 2000.

[14] F. Demmerle, W. Wiesbeck, '*A biconical multibeam antenna for space division multiple access*', IEEE Trans. Ant. Prop., Vol. 46, No. 6, June 1998, pp. 782-787.

[15] M. Feder, E. Weistein, '*Parameter estimation of superimposed signals using the EM algorithm*', IEEE Trans. Signal Proc., Vol. 36, No. 4, Apr 1988, pp. 477-489.

[16] B. H. Fleury, M. Tschudin, R. Heddergott, D. Dahlhaus, K. I. Pedersen, '*Channel parameter estimation in mobile radio environments using the SAGE algorithm*', IEEE JSAC, Vol. 17, No. 3, Mar 1999, pp. 434-449.

[17] C. C. Chong, D. I. Laurenson, C. M. Tan, S. McLaughlin, M. A. Beach, A. R. Nix, '*Joint detection estimation of directional channel parameters using the 2-D frequency domain SAGE algorithm with Serial Interference Cancellation*', conference proceeding in ICC 2002, New York City, Apr 28- May 2 2002.

[18] P. E. Hyberg, '*Circular to linear array mapping using calibrated data*', IEE Conf. HF Radio Systems and Techniques, 2000.

[19] A. Y. J. Chan, J. Litva, '*MUSIC and maximum likelihood techniques on two-dimensional DoA estimation with uniform circular array*', IEE Proc. Radar, Sonar, Navig., Vol. 142, No. 3, June 1995, pp. 105-113.

On the Application of Circular Arrays in Direction Finding Part II: Experimental evaluation on SAGE with different circular arrays

C. M. Tan[1,†], M. Landmann[2], A. Richter[2], L. Pesik[1], M. A. Beach[1], Ch. Schneider[2], R. S. Thomä[2], and A. R. Nix[1]

[1]Centre for Communications Research,
Dept. Electrical and Electronic Eng.,
University of Bristol,
Bristol BS8 1UB, UK.
Tel: +44 117 954 5202, Fax: +44 117 954 5206

[2]Technical University Ilmenau,
Dept. Communication and Measurement,
P.O. Box 100565,
98684 Ilmenau, Germany.
Tel: +49 3677 69 1157, Fax: +49 3677 69 1113

[†]Email: Chor.Min.Tan@bristol.ac.uk

ABSTRACT

The application of different circular arrays in direction finding or directional channel sounding is investigated experimentally in this paper. The optimised design of the geometry of a circular array that can enhance the performance of the SAGE algorithm in direction finding is presented. In particular, several circular arrays with different element types are considered, and their impact on data quality in directional channel estimation is studied through numerous test measurements conducted within an anechoic chamber. Our studies show that the performance of the SAGE algorithm varies between different arrays structures despite its freedom and flexibility in any arbitrary array geometry.

I. INTRODUCTION

In recent years several measurement techniques have been proposed in order to obtain channel information that enable the extraction of the direction-of-arrival (DoA) and direction-of-departure (DoD) information [1]. In order to retrieve the directional information from the measured data efficiently, the measurement equipment and post-processing tools must support the antenna arrays. Here, a state-of-the-art wideband vector channel sounder described in [2] suits this purpose well.

When a full 360º azimuth field of view is required, a uniform circular array (UCA) should be employed such that the full 360º channel responses can be recorded within the coherence time of the channel. This ensures that the instantaneous DoAs or DoDs of the multipaths at a particular time instant from all directions can be resolved within a measurement snapshot. Sub-optimal methods based on the linear arrays do not support this principle, since the real channel is multipath-rich and non-stationary [3]. If both the azimuth and elevation information are important, a 3-D array such as the spherical array proposed in [4] should be used. Since the main objective of this work is to study the performance of the Space-Alternating Generalised Expectation-Maximisation (SAGE) [5] algorithm using different UCAs, only the azimuth information is considered here.

In Part I [3], we show that the performance of the SAGE algorithm when applied to a UCA is superior to other algorithms, and this is justified analytically by means of comparison between the performance of several algorithms using a simplified data model. Potentially, the choice of the UCA used plays an important role in determining the actual performance of the SAGE when applied to real measured data from a real environment. From the mathematical and theoretical point of view, SAGE should work with any array configuration consisting of any arbitrary architecture as long as the exact array manifold knowledge is available. But, this is not always true since the performance of the SAGE relies on the array manifold pattern as well as the choice of the array element type. This constitutes the main reason that SAGE behaves differently with different arrays of the same geometry and dimension.

Having justified SAGE as the preferred algorithm for the UCA case in Part I [3], we investigate its performance with different UCAs in this paper – Part II. The organisation of Part II is follows. A study of the optimised array design that can improve the performance of SAGE is given in Section 2. Section 3 describes the different UCAs as well as the test procedure and the measurement setup for the experiments Section 4 discusses the initial measurement results produced by SAGE. Finally, Section 5 concludes this paper.

II. ENHANCING THE PERFORMANCE OF SAGE

First, we develop a simple narrowband data model and review the basic philosophy of the SAGE algorithm [5] as a precursor to the following discussions. Assuming a total of K signals from far field impinge on an N-element UCA, the UCA response is given by:

$$x(t)^{[Nx1]} = \sum_{k=1}^{K} s_k(t)^{[Nx1]} + \sigma n(t)^{[Nx1]} \quad (1)$$

where $$s_k(t)^{[Nx1]} = \gamma_k(t) a(\Theta_k)^{[Nx1]} \quad (2)$$

is the k-th signal component, $\gamma_k(t)$ is the complex path weight of the k-th signal at time t, $a(\Theta_k)$ is the UCA steering vector that depends on the direction $\Theta_k = (\theta_k,\phi_k)$ and is defined in eq. 2 in Part I [3], $n(t)$ is the complex noise that is independently and identically normal distributed with a standard deviation σ, and the superscript $[\cdot]$ denotes the dimension of the vector.

The basic principle of the SAGE algorithm is to minimise the following cost function:

$$\xi^2(x,\Theta) = (x - s(\Theta))^H \cdot (x - s(\Theta)) \quad (3)$$

where $s(\Theta) = \sum_{k=1}^{K} s_k$ is the summation of all the K signal components, and H denotes the Hermitian transpose operator. Minimising the cost function is a non-convex minimisation problem, since the cost function has one global minimum and several local minima. In the case of using the vector channel sounder as described in [2], some of the signals will be coherent, i.e. the signals impinge on the UCA are correlated as they are emitted from the same source and might have very similar Θ values. When coherent signals are present, the cost function (3) is likely to converge to its local minimum as a solution to the minimisation problem. This causes SAGE to produce the wrong estimates for the virtual paths (which are in fact non-existent).

The implementation of the SAGE is based on locating the peak in the correlation function:

$$c_k(x,\Theta) = x_k^H a(\Theta) \quad (4)$$

where x_k is the complete data of the k-th path [5] which is obtained in the expectation step (E-step) of the SAGE algorithm. The location of the peak corresponds to the value of the parameter of interest and is estimated in the maximisation step (M-step) of the SAGE algorithm. Note that this is the same principle as that in the EM algorithm [6]. However, for an m-dimensional (m-D) estimation problem, EM algorithm has to perform K optimisation processes in the m-D space, whereas SAGE just has to perform $m*K$ optimisation processes separately in 1-D space.

The shape of the correlation function (4) depends on the nature of the k-th *complete data*, x_k, and the array pattern (i.e. the structure of the UCA). In the implementation of SAGE, x_k is computed in the E-step by using either the *Parallel Interference Cancellation* (PIC) or the *Serial Interference Cancellation* (SIC) technique, represented by (5) and (6), respectively:

$$x_{k,PIC} = x - \sum_{\substack{l=1 \\ l\neq k}}^{K} \hat{s}_l \quad (5)$$

$$x_{k,SIC} = x - \sum_{l=1}^{k-1} \hat{s}_l \quad (6)$$

where $\hat{s}_l$ is the estimated signal copy of the l-th path. Note that since $\hat{s}_l$ is only the estimated value, not all the contributions from the previous estimated paths are subtracted from x. Hence, x_k contains the wanted information of the k-th path as well as the unwanted residue information from other paths.

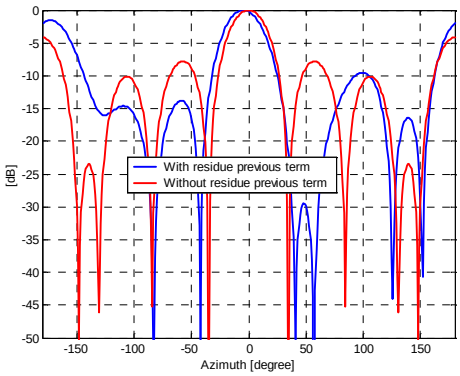

Figure 1 Correlation function for the k-th path ϕ_k = 0º, 8-element omni-directional UCA, r = r_{max}

Figure 1 shows the correlation function for the k-th path, ϕ_k = 0º. When the residue terms from -15º and 60º are not fully removed from x_k. c_k peaks at -5º with a high sidelobe at -175º. When the residue terms are fully removed, c_k peaks at 0º and the sidelobe level is lower. In the worst case, if the sidelobes corresponding to the k-th path and the residue components are higher (due to constructive superposition) than the main lobe, a wrong estimate will be produced.

Since it is unlikely that all the residue components from other paths to be fully removed from x_k in an estimation process, we can minimise the probability of estimating the wrong results by reducing the sidelobe level in the correlation function. This can be achieved by using a UCA with a radius smaller than its maximum value (7) [3]

$$r_{\max} = \frac{N\lambda}{4\pi} \quad (7)$$

where λ is the wavelength. Through extensive numerical simulations, the optimum radius that can enhance the performance of SAGE is found to be

$$r_{opt} \approx \frac{N\lambda}{16} < r_{\max} \quad (8)$$

such that the corresponding mainlobe and the sidelobes in c_k have the largest separation.

Figure 2 shows the c_k function for ϕ_k = 0º and for different radius (details in caption). In general, c_k should decrease monotonically and $r<r_{max}$ serves this purpose well. Clearly, the sidelobes when $r<r_{max}$ are lower than that of $r=r_{max}$. The problem becomes worse when the spatial Nyquist sampling theorem is violated when $r=2\lambda>r_{max}$. Figure 3 shows the improvement achieved when $r=r_{opt}$ is used for the same problem associated with the discussion in Figure 1.

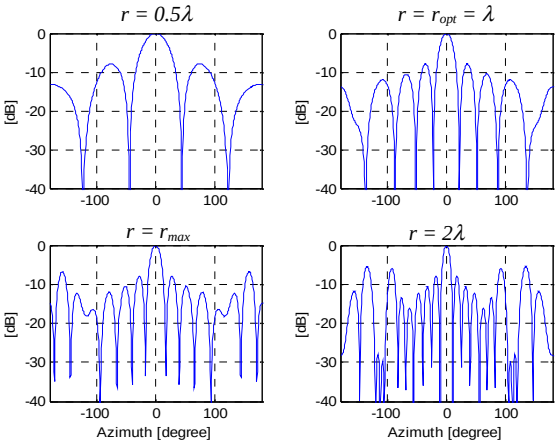

Figure 2 Correlation functions for the k-th path ϕ_k = 0º, 16-element omni-directional UCA

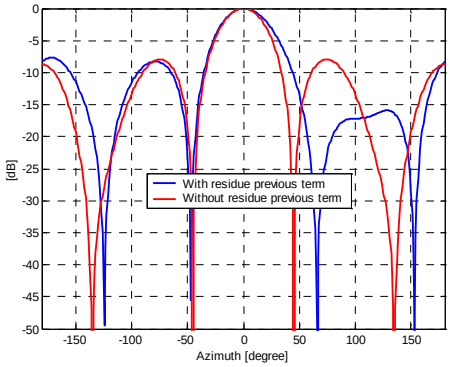

Figure 3 Correlation function for the k-th path ϕ_k = 0º, 8-element omni-directional UCA, r = r_{opt}

In addition, further enhancement can be made by using the directional elements. This is shown in Figure 4 where the sidelobes are further attenuated monotonically. In this case, the probability of producing an estimation error due to the contributions of the residue components in x_k is greatly minimised.

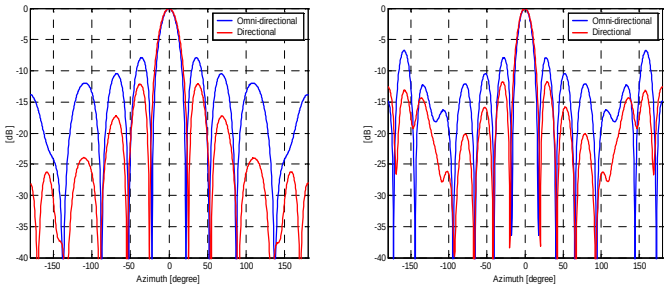

Figure 4 Correlation function for the k-th path, ϕ_k = 0º, N = 16
——— omni-directional elements, ——— directional elements

Thus, with an optimised array geometry, its resultant optimised beampattern will produce a more 'well-shaped' pattern in the correlation function and can maximise the probability of the cost function (3) converging to its global minimum, and the probability of estimating the virtual paths can be further reduced.

III. DESCRIPTIONS OF THE UCAs AND MEASUREMENT PROCEDURE

A. *Different UCAs used in the experiments*

In order to evaluate the performance of SAGE on different UCAs in a more realistic way, several 8-element UCAs of the same radius[1], $r = 0.64\lambda$, with different element types were constructed. The UCAs were designed to operate in the 5.2 GHz band. Figure 5 shows the pictures of:

a. Vertical polarisation uniform circular monopole array (UCMA)
b. Dual polarisation uniform circular patch array
   i. Horizontal polarisation (HP-UCPA)
   ii. Vertical polarisation (VP-UCPA)
c. Horizontal polarisation uniform circular dipole array (HP-UCDA)
d. Vertical polarisation uniform circular dipole array (VP-UCDA)

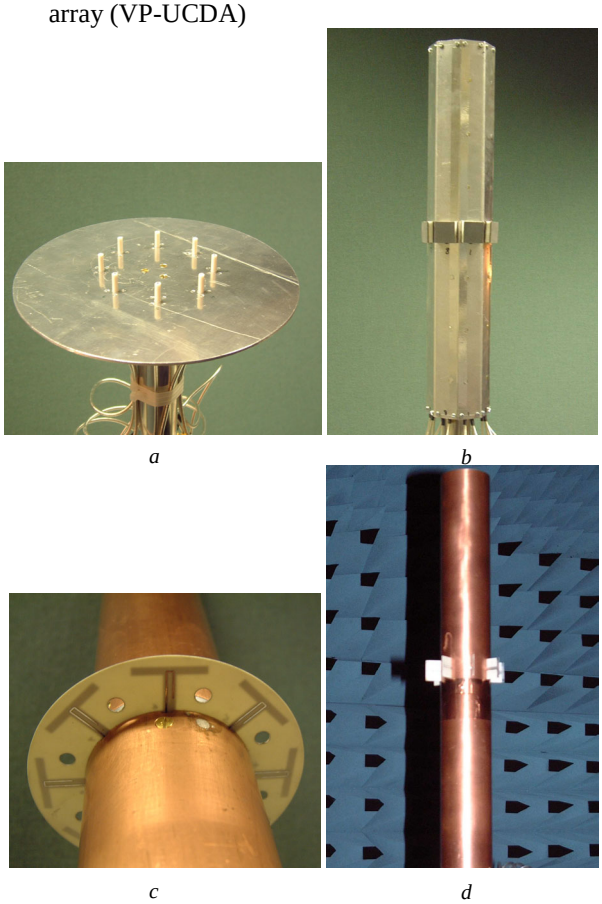

a - 8-element vertical polarisation monopole array (UCMA)
b – 8-element dual-polarisation patch array
horizontal polarisation (HP-UCPA)
vertical polarisation (VP-UCPA)
c – 8-element horizontal polarisation dipole array (HP-UCDA)
d – 8-element vertical polarisation dipole array (VP-UCDA)

Figure 5 Pictures of different UCAs

[1] These UCAs were constructed at the beginning of this project and hence the radius had been designed to be equal to r_{max} in (7). However, if any new UCA were to be constructed for directional channel sounding purpose in future, we would prefer to use r_{opt} in (8) instead of r_{max} in (7).

The length of the monopoles in the UCMA is $\lambda/4$. The elements used in the patch array are the dual-polarised circular stacked patch antennas [7], and for that in the HP-UCDA and VP-UCDA are the printed dipoles of length equal to $\lambda/2$. All elements in the arrays (except UCMA) are mounted in the middle of a cylindrical ground plate. The length of both the upper and lower parts of the cylindrical ground plate was chosen to be 5λ in order to minimise the undesirable edge fringing effect. Each of the printed dipoles is displaced by $\lambda/4$ from the cylindrical ground plate (figure 6) to reduce the destructive superposition of the impinging waves – Image theory [8].

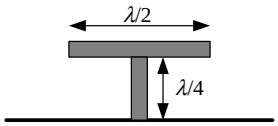

Figure 6 The dimension of the printed dipole

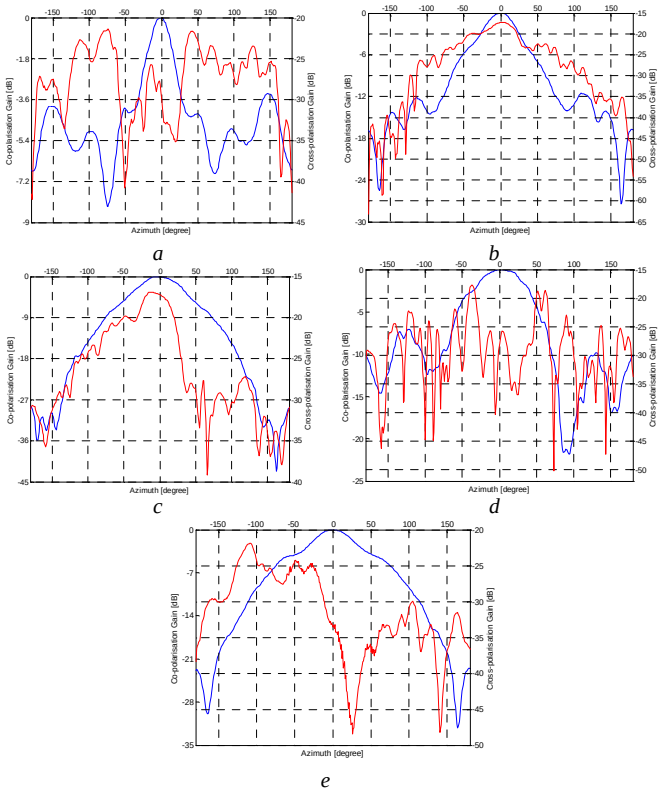

a – UCMA, b – HP-UCPA, c – VP-UCPA
d – HP-UCDA, e – VP-UCDA
co-polarised pattern (left vertical axis)
cross-polarised pattern (right vertical axis)

Figure 7 Measured beampatterns for an example element on the UCAs, all plots are normalised to the peak in the co-polarised gain

Figure 7 (details in caption) shows the co-polarised and cross-polarised radiation patterns for an example element on the UCAs, measured in an anechoic chamber using the Wiltron Network Analyser. The radiation patterns are asymmetric due to the effects of mutual coupling and the array imperfections, since spatial calibration process (similar to that in [9]) has not been applied to the UCAs as yet. It can also be seen that surface waves exist on the UCAs (except UCMA) and propagate round the cylindrical ground plate since the responses are not zero when the orientation of the UCAs (except UCMA) is at –180º (or 180º). The 10λ long cylindrical ground plate for the vertically polarised arrays has caused their elements to exhibit a wider co-polarised beamwidth.

B. *Measurement setup*

The measurements were conducted in an anechoic chamber at 5.2 GHz using a Medav RUSK BRI channel sounder (similar to that in [2]). All the UCAs were set to be the receiver. The transmitter was a dual-polarised commercial horn antenna. At 5.2 GHz, its gain was 11.5 dBi and its 3-dB beamwidth in the *E-plane* and *H-plane* was 40º and 35º, respectively. The transmitted periodic multi-frequency test signal had a bandwidth of 120 MHz with 0.8 μs repetition period window, and was set to be co-polarised with the UCA under consideration. The tests[2] that were conducted are as follows.

a. *2 coherent sources tests*

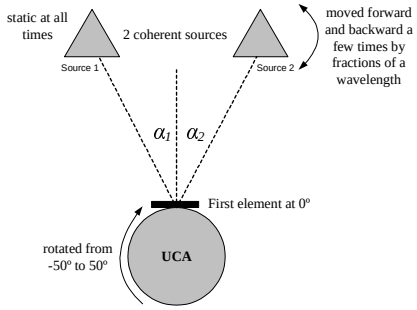

Figure 8 Sketched plan for the 2 coherent sources test

The UCA was fixed in the middle and its orientation was rotated from -50º to 50º in 10º steps. The 2 coherent sources were placed at an angle equally away from both sides of the UCA centre axis, i.e. $\alpha_1 = \alpha_2$. The first coherent source was static at all times, while the second one was moved forward and backward by a small fraction of a wavelength several times for each of the UCA's orientations. The reason for this was to collect a few samples in which the phase offset for the 2 coherent sources was different in each sample. In all measurements, the UCA and the 2 coherent sources were set the same height.

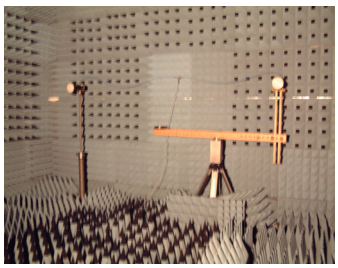

Figure 9 The 2 coherent sources test

[2] Due to limited time constraints, not all tests were performed using all UCAs.

b. LOS measurement with different TX-RX heights

The purpose of this test is to evaluate the impact of neglecting the elevation angle in direction finding. Both the TX and the UCA were set at different heights and directly faced each other. Measurements were taken for each UCA's orientation from -180° to 180°.

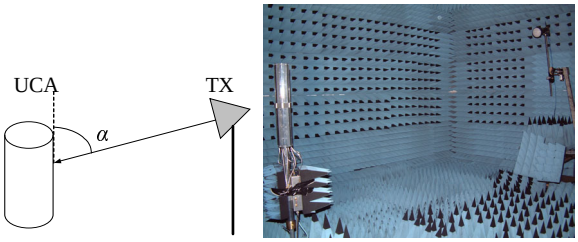

Figure 10 The elevation test

IV. PERFORMANCE EVALUATION

One of the most useful tests to determine the effectiveness and robustness of the algorithm is the coherent source test. Although the UCAs have the similar geometry, their results behave differently in the presence of coherent sources. The performance of the SAGE algorithm on different UCAs is evaluated in this section, based on the initial results obtained so far. Since this is a wideband measurement and the measurement data was stored as the complex frequency response, we have used the 2-D SAGE algorithm to estimate the DoA and the time-delay-of-arrival (TDoA) together. Due to space constraint, not all results are shown here.

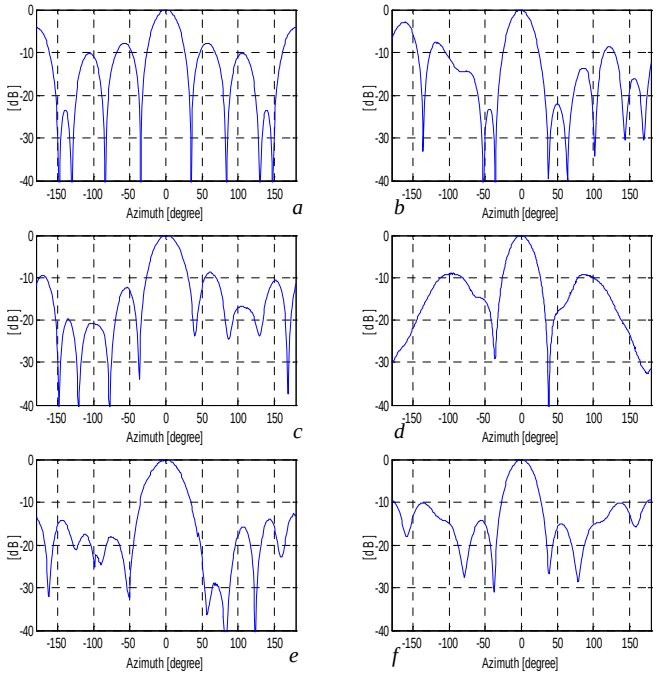

a – Ideal monopole, N = 8, r = r_{max}, *b - UCMA*
c – HP-UCPA *d – VP-UCPA*
e – HP-UCDA *f – VP-UCDA*

Figure 11 Correlation functions for the UCAs, ϕ = 0°

First, we examine the correlation function of the UCAs when ϕ = 0° (Figure 11). As mentioned in Section 2, by using the elements with directional beampattern, the sidelobe level in the correlation function can be further reduced. This observation is confirmed by comparing the real correlation functions of different UCAs (except UCMA) with that of an ideal omni-directional UCA. By inspection, we would expect the performance of the VP-UCPA to be superior to others since its correlation function is the most 'well-shaped' here. The sidelobes of other correlation functions do not roll off monotonically and this might affect the accuracy of the estimated results. But this is inconclusive at this stage and further tests must be performed to confirm this.

The correlation functions are very different to each other since the elements of each UCA are different. Moreover, they are not symmetrical partly due to the different degrees of mutual coupling and array imperfections within themselves, as well as (possibly) minor technical faults occurred during the measurements (e.g. the vertical axis of the UCAs was not exactly aligned with the axis of rotation of the mounting device in the anechoic chamber). In the following sections, the DoAs were estimated using the measured array manifold in the 2-D SAGE correlation process, and no spatial calibration has been applied as yet. The resolution of the spatial sampling grid of the measured array manifold is 1°. Thus, the following estimation is performed by using the discrete data model at a correlation grid of 1°.

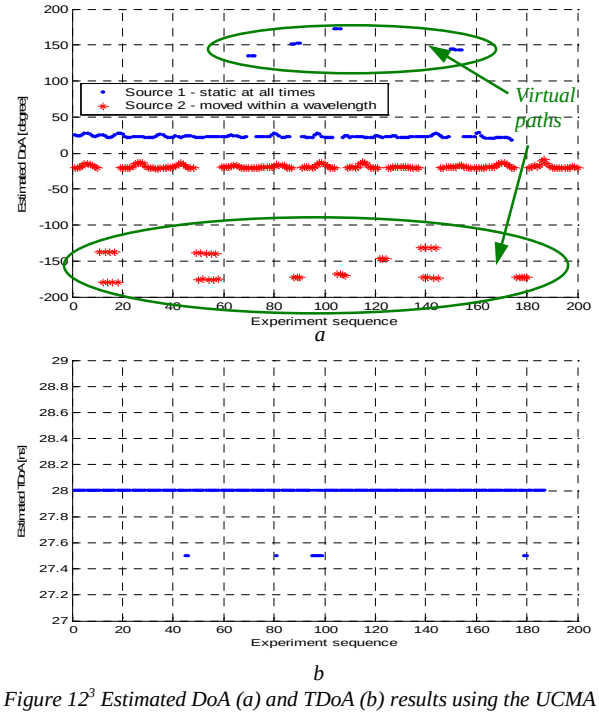

Figure 12[3] Estimated DoA (a) and TDoA (b) results using the UCMA

[3] All the estimated DoA results are plotted after normalising their absolute values to the UCA orientation with respect to the centre axis (Figure 8), i.e. only the estimated α_1 and α_2 values are plotted here.

Figure 12a shows the estimated DoAs for the 2 coherent sources separated by (approximately) 40º using the UCMA. Most of the times the 2 coherent sources are separable but SAGE produces some wrong estimates for the virtual paths occasionally. The main reason for this is due to the bad constellation of the path weights of the 2 coherent sources that results in constructive superposition of the sidelobes and destructive superposition in the actual mainlobe in the correlation function. Since one of the coherent sources was moved forward and backward within fractions of a wavelength in each experiment sequence (Figure 8), different samples of path weights constellation were obtained since the phase difference between the paths was different. Unreliable estimates will be obtained when the critical path weights constellation occurs. However, the estimated TDoA (Figure 12b) is very accurate since it relies on the temporal correlation function which exhibits a much better behaviour than the spatial correlation function (due to the large sounding bandwidth of 120 MHz).

In addition, using the UCMA of this type in directional channel sounding has one major disadvantage compared to other UCA topologies. When the sources are not co-planar with the UCMA, the ground plate of the UCMA will act as a reflector to the impinging waves (i.e. scattering on the ground plate) and causes the array response to be distorted. The degree of distortion determines the degree of modification on the phase shift between the elements needed in the DoA estimation process. A wrong estimate will be produced when SAGE is not able to cope with the distortion that has corrupted the phase shift information on the UCMA. This effect is not observable here since the UCMA and the coherent sources were co-planar, i.e. at the same height.

Figure 13 shows the estimated DoAs of the 2 coherent sources separated by 40º with the HP-UCDA (a) and HP-UCPA (b). The results are a little biased (for Source 2) and wrong estimates occur occasionally (for HP-UCDA). We believe this is caused by the bad path weights constellation of the two sources. Better improvement could be achieved if the reference data (the measured manifold) has a better resolution, i.e. the step size of the spatial correlation sampling grid is less than 1º. In a coherent case, the degree of accuracy also depends on the degree of separation between the sources. This is demonstrated in Figure 14 where the estimated results with HP-UCDA (a) and HP-UCPA (b) are better when the sources were separated by 50º. Results also show that the HP-UCPA is superior to HP-UCDA since the latter produced estimation errors occasionally.

Table 1 shows the standard deviation of the estimated DoAs of the 2 coherent sources without including the wrong estimates. The standard deviation for Source 1 is always lower than that for Source 2 since Source 1 was static at all times and Source 2 was moved forward and backward several times for each UCA orientation (Figure 8). Results from HP-UCPA have a smaller standard deviation than that of HP-UCDA, and the standard deviation is also smaller when the sources were separated further apart.

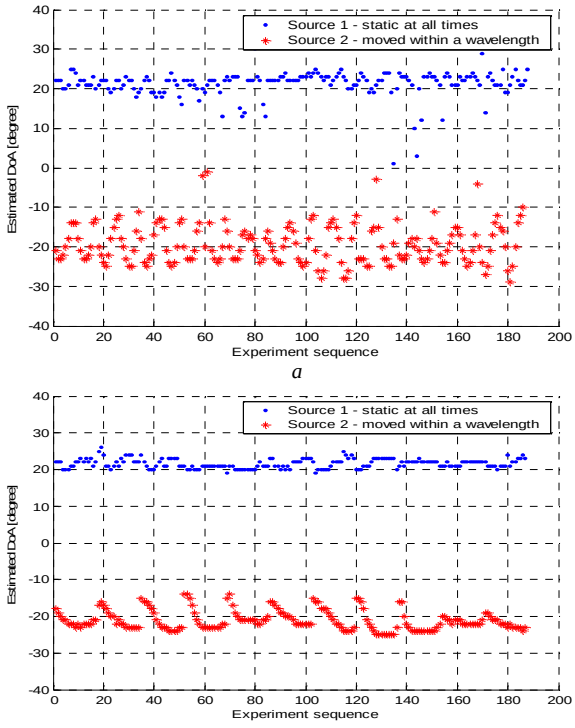

Figure 13[3] Estimated DoA results for the 2 coherent sources separated by 40º using the HP-UCDA (a) and HP-UCPA (b)

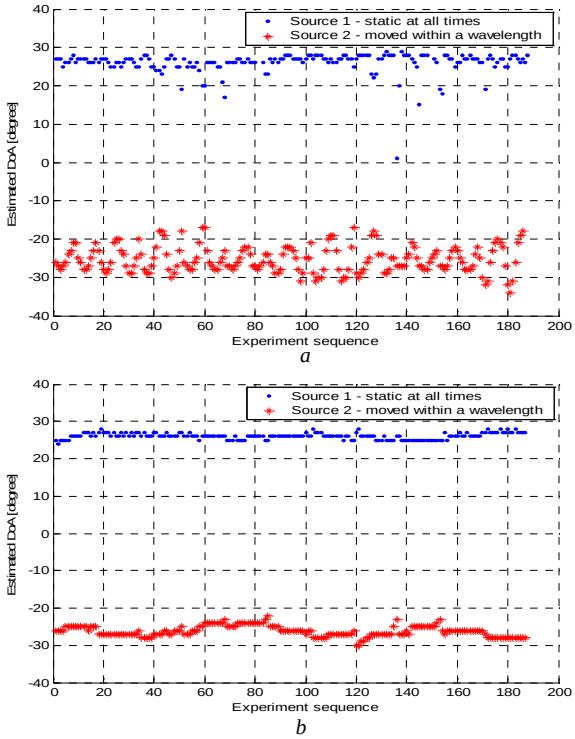

Figure 14[3] Estimated DoA results for the 2 coherent sources separated by 50º using the HP-UCDA (a) and HP-UCPA (b)

UCAs	Coherent sources separation	Standard deviation	
		Source 1	Source 2
UCMA	40º	0.8º	1.9º
HP-UCDA	40º	3.3º	4.9º
HP-UCDA	50º	3.0º	3.5º
HP-UCPA	40º	1.2º	2.7º
HP-UCPA	50º	0.8º	1.4º
VP-UCPA	40º	0.9º	1.3º
VP-UCPA	50º	0.6º	1.0º

Source 1 refers to α_1 in Figure 8 (the upper part of the estimated DoA graphs), Source 2 refers to α_2 in Figure 8 (the lower part of the estimated DoA graphs).

Table 1 Standard deviation of the estimated DoAs of the 2 coherent sources (without including the virtual paths)

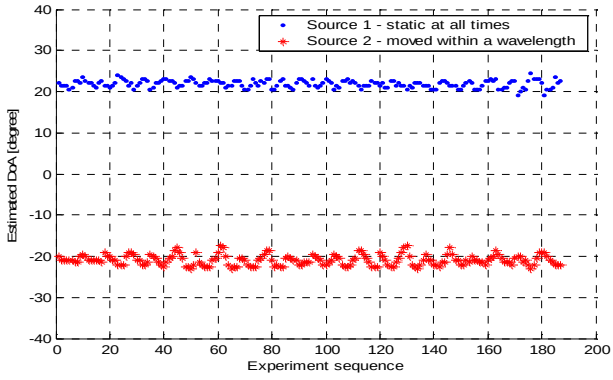

a

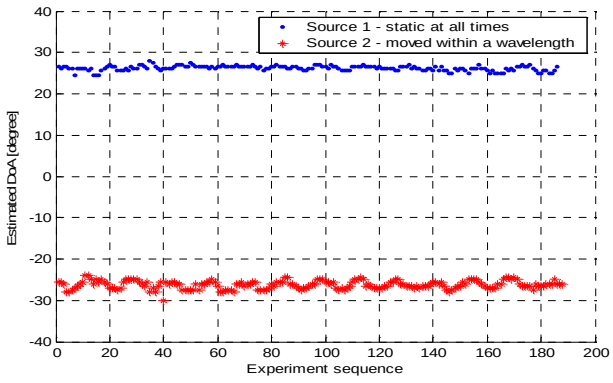

b

Figure 15[3] Estimated DoA results of the 2 coherent sources separated by 40º (a) and 50º using the VP-UCPA

Figure 15 shows the estimated DoA results for the 2 coherent sources separated by 40º (a) and 50º (b) with the VP-UCPA. In contrast to the previous estimation, the results obtained using the VP-UCPA were produced with a spatial correlation sampling grid of 0.5º. Amongst all the UCAs, VP-UCPA seems to produce the best results. The estimated results are consistent and have the smallest standard deviations. Results of Source 2 seem to be a little 'oscillatory' since it was moved forward and backward several times for each UCA orientation (so that different phase offsets of the signals can be obtained). The fluctuation in the DoA results corresponding to Source 2 has demonstrated some sort of periodicity and this implies that the SAGE is able to track little changes in the DoA when Source 2 was moved in that manner. The improvement presented in Figure 15 is achieved since the reference data of the VP-UCPA has a better resolution (0.5º) compared to the reference data of other UCAs (1º grid).

All the estimated results shown above do not match the expected angular displacement of the 2 sources (40º or 50º) hints that the sources are not separated by exactly 40º or 50º apart during the measurement. This is inevitable although every effort has been made to minimise any source of errors during the experiments. Moreover, the path weights constellation in all experiments is also different since the exact positions of the sources were altered whenever a new experiment was conducted. The number of SAGE iterations used here is between 5-50 times. Note that as the separation distance of the sources decreases, more iterations will be needed to achieve convergence. A reference data with a smaller sampling grid (ideally continuous) should be used if better accuracy were to be achieved.

Figure 16 shows the results of the elevation test using the VP-UCPA. The single source was elevated at an angle of about 12º from the azimuth plane and the results were produced by neglecting the elevation angle. It shows that the performance of the SAGE is unaffected at this elevation angle since the estimates are very accurate. However, we would expect the results to be more biased as the elevation angle of the source increases. Due to the limited physical size of the anechoic chamber, not much elevation tests (for a source at far field) could be performed to confirm this. Although the UCA is able to produce some sort of elevation angle information, it might not be reliable due to the limited beamwidth of the elements on the UCA. In order to obtain both azimuth and elevation angles properly, a 3-D array such as that proposed in [4] should be used.

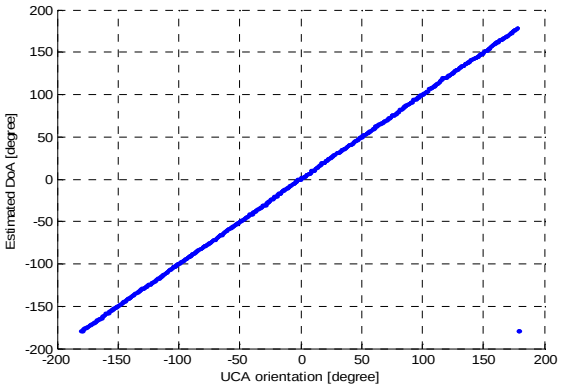

Figure 16 Results of elevation test using the VP-UCPA

V. CONCLUSION

The performance of the SAGE algorithm using different UCAs is evaluated based on different experiments conducted in an anechoic chamber. Since the results corresponding to different UCAs vary among themselves, it can be concluded that the measurement outcome is dependent on the array choice. Although no further conclusion on the 'best array element choice' can be drawn as yet but the work presented here provides a good indication that the VP-UCPA is able to produce the best estimation results. It is expected that the performance of the SAGE algorithm using the optimum array design discussed in Section 2 would further enhance the performance.

Results show that in the presence of the coherent sources, UCMA is not able to provide reliable DOA estimates. Improvement could be obtained if the optimum array radius (r_{opt}) is used. However, the ground plate of the UCMA might cause wrong estimation results when the sources are not co-planar with the array – a phenomena that is unavoidable in real environment. This implies that the UCMA is not suitable in directional channel sounding. On the other hand, the TDoA estimates are very accurate in all cases since it is unaffected by the array structure.

Note that the work presented so far has not excluded the effects of the mutual coupling in the UCAs. It is expected that by performing the spatial calibration process (similar to that in [9]) prior to applying the algorithm would further enhance the performance. With that, a smaller sampling grid in the correlation process can be used and the results will be more accurate. Research is now on-going to develop a calibration algorithm that is suitable for the UCAs.

Since the performance of SAGE varies between different arrays and it is important to exclude any effect of the antenna from the propagation channel [1], a proper array that is suitable for directional channel sounding must be carefully chosen.

ACKNOWLEDGEMENT

The authors would like to acknowledge Dr. D. L. Paul and Mr. K. Steven (both at Bristol Uni.) for their contributions in designing and constructing the UCAs, and the Mobile VCE (www.mobilevce.com) for the financial support of Chor Min Tan.

REFERENCES

[1] M. Steinbauer, A. F. Molisch, E. Bonek, '*The Double-directional radio channel*', IEEE AP Magazine, Vol. 43, No. 4, Aug 2001.

[2] R. S. Thomä, D. Hampicke, A. Richter, G. Sommerkorn, A. Schneider, U. Trautwein, and W. Wirnitzer, '*Identification of time-variant directional mobile radio channels*', IEEE Trans. Instrum. and Meas., Vol. 49, Apr 2000, pp. 357–364.

[3] C. M. Tan, P. Fletcher, M. A. Beach, A. R. Nix, M. Landmann, R. S. Thomä, '*On the application of circular arrays in direction finding, Part I: Investigation into the estimation algorithms*', companion paper in 1st Annual COST 273 Workshop, Espoo, Finland, May 29-30, 2002.

[4] K. Kalliola, '*Experimental analysis of multi-dimensional radio channel*', PhD. Thesis, Helsinki University of Technology, 18 Sept 2001.

[5] B. H. Fleury, M. Tschudin, R. Heddergott, D. Dahlhaus, K. I. Pedersen, '*Channel parameter estimation in mobile radio environments using the SAGE algorithm*', IEEE JSAC, Vol. 17, No. 3, Mar 1999, pp. 434-449.

[6] M. Feder, E. Weistein, '*Parameter estimation of superimposed signals using the EM algorithm*', IEEE Trans. Signal Proc., Vol. 36, No. 4, Apr 1988, pp. 477-489.

[7] D. L. Paul, I. J. Craddock, C. J. Railton, P. N. Fletcher, M. Dean, '*FDTD analysis and design of probe-fed dual-polarised circular stacked patch antenna*', Microwave and Optical Tech. Letters, Vol. 29, No. 4, May 2001, pp. 223-226.

[8] C. A. Balanis, '*Linear elements near or on infinite perfect conductors*', Chapter 4 in Antenna Theory, Analysis and Design, 2nd Edition, John Wiley and Sons, 1997.

[9] G. Sommerkorn, D. Hampicke, R. Klukas, A. Richter, A. Schneider, R. Thomä, '*Reduction of DoA estimation errors caused by antenna array imperfections*', 29th Euro. Microwave Conf., Munich, Oct 5-7, 1999.